



Understanding the escape of water from Enceladus

M. H. Burger,¹ E. C. Sittler Jr.,¹ R. E. Johnson,² H. T. Smith,² O. J. Tucker,²
and V. I. Shematovich³

Received 15 September 2006; revised 21 November 2006; accepted 4 January 2007; published 14 June 2007.

[1] On 14 July 2005, Cassini passed within 175 km of Enceladus' surface enabling a direct in situ measurement of water escaping from the surface by the Ion and Neutral Mass Spectrometer (INMS) and the observation of a stellar occultation by the Ultraviolet Spectrometer (UVIS). We have developed a three-dimensional, Monte Carlo neutral model to simultaneously model the INMS and UVIS measurements of water gas density and column density, respectively. The data are consistent with a two-component atmosphere; the first with a weak, distributed source on the surface which, if global, has a source rate of $\sim 8 \times 10^{25}$ H₂O/s, and the second with a much larger source localized at the south pole with a source rate $\sim 10^{28}$ H₂O/s. This latter source is possibly coincident with the "tiger stripe" series of fractures revealed by the Imaging Science Subsystem instrument where the ice was measured to be warmer than the surrounding regions by the Composite Infrared Spectrometer instrument. We estimate the plasma mass loading rate due to interaction between the plume and magnetospheric plasma is 2–3 kg/s for a plume source of 10^{28} H₂O/s. Pickup of water group ions in the plume slows down the plasma to ~ 10 km/s relative to Enceladus in the region of, and downstream of, the south polar plume. This is consistent with the mass loading rate inferred from magnetic field perturbations detected during the Cassini flyby and suggests an additional source may be needed to explain the plasma flow deflections detected by the Cassini Plasma Spectrometer.

Citation: Burger, M. H., E. C. Sittler Jr., R. E. Johnson, H. T. Smith, O. J. Tucker, and V. I. Shematovich (2007), Understanding the escape of water from Enceladus, *J. Geophys. Res.*, *112*, A06219, doi:10.1029/2006JA012086.

1. Introduction

[2] The discovery of active volcanism at the small icy moon Enceladus has been one of the great unexpected discoveries of the Cassini/Huygens mission to Saturn. Although it was known from Earth-based observations that Saturn's inner magnetosphere is dominated by water group neutrals associated with the icy satellites (as reviewed by Richardson [1998]), and the principle source of these neutrals had been shown to be close to the orbit of Enceladus [Jurac *et al.*, 2002], the dramatic nature of the water source was a great surprise. In this paper we examine the strength of the water gas source at Enceladus and estimate the effect of the Enceladus plume on the magnetospheric plasma.

[3] The first confirmed detection of water dissociation products in Saturn's magnetosphere was made by Shemansky *et al.* [1993], who detected a neutral OH cloud using the "Hubble Space Telescope" (HST). Follow-up observations

[Hall *et al.*, 1996] confirmed the presence of a substantial OH cloud with peak densities ~ 700 cm⁻³ located at ~ 4.5 Saturnian radii (R_{Sat}) from Saturn, just outside of the orbit of Enceladus at $4 R_{\text{Sat}}$. Richardson *et al.* [1998] developed a two-dimensional model of the neutral distribution based on these observations. They describe an azimuthally symmetric OH cloud with density in the equatorial plane greater than 5 cm⁻³ between 1.5 and 11.5 R_{Sat} . Subsequent HST observations and modeling showed that the principle source was close to the orbit of Enceladus [Jurac *et al.*, 2002; Jurac and Richardson, 2005]. Recently, Johnson *et al.* [2006] have shown that this cloud forms from charge exchange between molecules in a narrow H₂O neutral torus centered at Enceladus and water product ions in the subcorotating magnetospheric plasma.

[4] Models of the expected sputtering rates from the icy satellites [e.g., Shi *et al.*, 1995; Jurac *et al.*, 2001] lead to the conclusion that satellite sputtering by magnetospheric ions and solar UV photons is an insufficient source mechanism by an order of magnitude. In addition, micrometeorite impact erosion of the main rings [Pospieszalska and Johnson, 1991] produced a cloud with the incorrect spatial morphology. Jurac *et al.* [2002] proposed a model suggested earlier by Johnson *et al.* [1989] in which the principle source was sputtering of small ice grains coorbiting with Enceladus. Jurac and Richardson [2005] extended the work by Richardson *et al.* [1998] and Jurac *et al.* [2002], finding a

¹Goddard Space Flight Center, NASA, Greenbelt, MD, USA.

²University of Virginia, Charlottesville, Virginia, USA.

³Department of Stellar Physics and Evolution, Institute of Astronomy, Russian Academy of Sciences, Moscow, Russia.

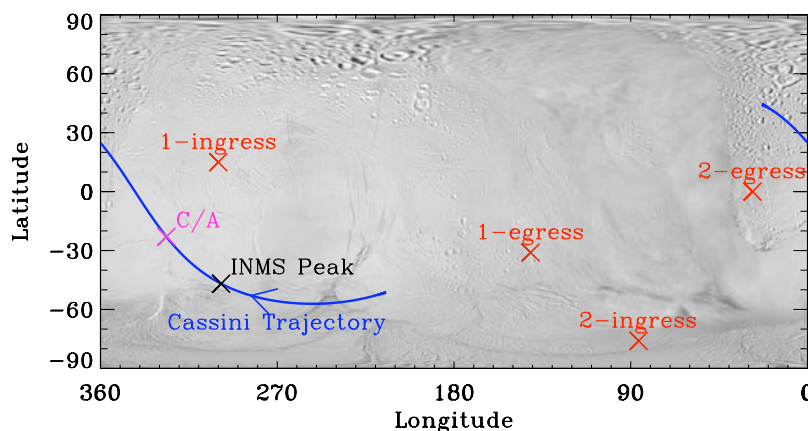


Figure 1. Map of Enceladus' surface showing the subspacecraft position during the 14 July 2005 flyby (blue), the location of the INMS peak water density (black), and the ingress and egress points for the two stellar occultations observed by UVIS (red).

source strength of $\sim 10^{28}$ molecules/s is required to explain the observations, an order of magnitude larger than previous estimates. In addition, the principal source region was found to be in the region of Enceladus' orbit.

[5] Predictions for mass loading of the plasma near Enceladus were made by *Sittler et al.* [2004] and *Saur and Strobel* [2005]. *Sittler et al.* [2004], using the sputtered neutral atmosphere calculated by *Jurac et al.* [2001], estimated the ion pickup that would be observed by Cassini Plasma Spectrometer (CAPS) during targeted flybys of Enceladus and Dione. Their sputtering model predicted a neutral surface density of a few times 10^5 cm^{-3} at each satellite, with pickup ion densities of ~ 2 and $\sim 1 \text{ cm}^{-3}$ at Enceladus and Dione, respectively. On the basis of calculated sputtering rates [*Jurac et al.*, 2001] and estimates of the plasma conditions measured by *Voyager*, *Saur and Strobel* [2005] predicted a surface column density at Enceladus of $6 \times 10^{11} \text{ cm}^{-2}$ with negligible ion production and mass loading. Each of these studies expected an extremely tenuous atmosphere with little detectable effect on the plasma signatures. Therefore it was a surprise when the Cassini Magnetometer (MAG) detected the bending of field lines near Enceladus because of the interaction with freshly created pickup ions [*Dougherty et al.*, 2006; *Kivelson*, 2006], and *Smith et al.* [2005] noted that the region near Enceladus' L shell appeared to be a source of nitrogen.

[6] To further understand the nature of the sources at Enceladus, Cassini made a close encounter on 14 July 2005 passing within 175 km of the surface. Observations by multiple instruments confirmed the presence of a strong source of water at the south pole of Enceladus.

[7] Direct observations of water vapor (as opposed to water ice grains or dust in the plume) were made by the Ion and Neutral Mass Spectrometer (INMS) [*Waite et al.*, 2006] and Ultraviolet Spectrometer (UVIS) [*Hansen et al.*, 2006]. Several features apparent in these data suggest a nonuniform source of water escaping from Enceladus. First, as noted by *Waite et al.* [2006], the peak in water density is not at the closest point to the surface along the Cassini flyby trajectory. The water cloud, therefore, is not symmetric about Enceladus as would be expected for a uniform source.

The peak is, however, symmetric about the south pole. The maximum density is coincident with the closest approach to the south pole, suggesting a source located there. Second, the peak density appears in the data as an order of magnitude spike on top of a slowly increasing background cloud with respect to the center of Enceladus. The full width half maximum of this peak is ~ 30 s, during which time Cassini traveled ~ 250 km. This is roughly the resolution limit of INMS near closest approach and is therefore qualitatively consistent with the narrow plumes observed by Imaging Science Subsystem (ISS) [*Porco et al.*, 2006].

[8] The path of the Cassini trajectory relative to the surface of Enceladus is shown in Figure 1. The farthest south the spacecraft footprint reached was -57° latitude. The closest approach to the satellite occurred over the point -23° latitude and 326° west longitude. The maximum water densities were measured near the southernmost part of the flyby. If the plume is confined to the south polar region, then the spacecraft did not fly directly over the source region, although molecules ejected tangentially to the surface could intersect the spacecraft trajectory.

[9] Cassini has twice had the proper trajectory to observe stars as they were occulted by Enceladus [*Hansen et al.*, 2006]. Measurements with UVIS' high-speed photometer and far ultraviolet spectrograph were designed to detect both the attenuation and absorption signatures of atmospheric constituents. The first occultation on 17 February 2005 of the star λ Scorpii showed no evidence of an atmosphere. The second occultation, however, of γ Orionis on 14 July 2005, showed water absorption lines during the stellar ingress. Neither attenuation nor water absorption were detected after egress. The ingress during this occultation occurred near Enceladus' south pole at a latitude of -76° and because of the observing geometry, measured material even closer to the pole. The other three surface intercept points were closer to the equator. The column density of water over the south pole as reported by *Hansen et al.* [2006] drops off $\sim r^{-3.1}$, significantly faster than the r^{-1} dependence expected for a nongravitationally bound exosphere escaping from the surface. This implies that the

stellar occultation measured a slice through a spatially nonuniform plume or that a significant fraction of the water vapor is gravitationally bound to Enceladus and returns to the surface.

[10] The injection of a large number of neutral atoms into the magnetosphere affects the ambient plasma and the magnetic field. Ionization of water molecules and charge exchange between H₂O and magnetospheric ions create fresh ions which are picked up by the magnetosphere. Both the CAPS [Tokar *et al.*, 2006] and MAG [Dougherty *et al.*, 2006] experiments detected mass loading through the effects of ion pickup. CAPS detected strong deflections in the plasma flow within 27 R_{En} from the satellite. On the basis of the perturbation to the flow, a mass loading rate of 100 kg/s has been inferred [Tokar *et al.*, 2006; Pontius and Hill, 2006]. The magnetometer measured the draping of field lines caused by interaction with the south polar plume. A mass loading rate of ~2 kg/s is sufficient to explain the magnitude of the magnetic signature [Khurana *et al.*, 2007].

2. Modeling the Water Distribution Near Enceladus

[11] We use a Monte Carlo model [Burger, 2003; Burger and Johnson, 2004] to understand the nature of the water vapor measured by Cassini. Packets are ejected from the surface with specified velocity and spatial distributions. The motion of each packet is followed under the influence of gravity from Saturn and Enceladus; the influence of the other satellites is negligible on the relevant timescales. The content of packets are decreased through interaction with the magnetospheric plasma as well as dissociation and ionization by solar UV radiation. Packets are removed from the simulation when they collide with satellites, Saturn's main rings, or Saturn itself.

2.1. Atmospheric Sources

2.1.1. Localized Source

[12] The primary source of water at Enceladus is the south pole plume. The plume consists of water in both gaseous and solid states. Since the mechanism responsible for the plume is not understood, it is difficult to know the velocity of water vapor at the surface. The available observations can, however, help to constrain this parameter. At closest approach, Cassini was ~175 km from the surface of Enceladus, and water was detected at least 1000 km from the surface. The velocity required to eject a water molecule upward from the surface of Enceladus to a distance of 1000 km is 225 m/s, slightly less than the escape velocity of 250 m/s. It seems probable, therefore, that a significant fraction of water in the plume escapes entirely from Enceladus. We adopt a Gaussian velocity distribution in the form

$$F(v, \theta) \propto e^{-\frac{(v-v_m)^2}{2\sigma_v^2}} \cos \theta \quad (1)$$

where $v_m = 500$ m/s is the mean velocity, $\sigma_v = 200$ m/s is the standard deviation of the distribution, and θ is the angle from the surface normal.

[13] The size of the source region is also not well constrained. The "south polar terrain," a region with unusual albedo and color features showing signs of recent tectonic activity, is southward of ~-55° latitude [Porco *et al.*, 2006]. This region includes the "tiger stripes," a family of roughly parallel features which appear to be the source of the ice grains. High-resolution temperature data obtained by the Composite Infrared Spectrometer (CIRS) experiment show that the tiger stripes are warmer than the surrounding regions, with temperatures 145 K [Spencer *et al.*, 2006]. In modeling the water vapor plume, we assume a source which is uniform over an area centered on the south pole. The size of the region is a free parameter in modeling the Cassini data.

2.1.2. Distributed Source

[14] The surface temperature is too low for sublimation of ice everywhere except for the small, anomalously warm regions inferred from CIRS data. Sputtering by energetic ions, however, is a possible mechanism known to produce distributed and, sometimes global, exospheres around planets and planetary satellites [Johnson, 1990] as have been observed at Mercury [Ip, 1986] and Europa [Brown and Hill, 1996; Hall *et al.*, 1995]. The sputtering rate at Enceladus has been estimated from pre-Cassini observations of the energetic particle flux to be ~10²⁵ H₂O/s [Jurac *et al.*, 2001], although the satellite sputtering rates are being revised by Cassini data. The primary sputtered product depends on the surface temperature; at Enceladus, the dominant species ejected is H₂O with smaller components of O₂ and H₂ [Johnson *et al.*, 2004]. In addition, the size of the yield depends on the micron-scale surface structure, so that freshly deposited surfaces have larger yields than surfaces which contain volatiles other than ice. Most of the material ejected from Enceladus' has sufficient energy to escape the satellite's gravitational pull and enter orbit around Saturn.

[15] Laboratory measurements show that the energy distribution of water molecules sputtered from an icy surface is given by:

$$F_{\text{H}_2\text{O}}^{\text{surface}}(E, \theta) \propto \frac{2EU_{\text{H}_2\text{O}}}{(E + U_{\text{H}_2\text{O}})^3} \cos \theta \quad (2)$$

where $U_{\text{H}_2\text{O}} = 0.055$ eV is the effective surface binding energy of H₂O, and θ is the angle normal to the surface [Johnson, 1990]. The most probable velocity of the sputter ejecta is 770 m/s, significantly larger than the escape velocity from Enceladus (250 m/s). Therefore 99% of the sputtered water escapes from Enceladus.

2.2. Neutral Loss Processes

[16] CAPS measured the plasma composition in the inner magnetosphere during Cassini's insertion orbit (Orbit SOI) [Young *et al.*, 2005; Sittler *et al.*, 2005a, 2006]. Sittler *et al.* [2005b] used these data, combined with Cassini/RPWS measurements of electron density [Persoon *et al.*, 2005], to solve the field-aligned force balance equations and calculate the plasma distribution as a function of magnetic L shell and latitude. The primary species in the plasma near Enceladus are protons (H⁺) and water group ions (O⁺, OH⁺, H₂O⁺, H₃O⁺, hereafter W⁺) with small amounts of O₂⁺ and N⁺ [Sittler *et al.*, 2005a]. In the magnetic equatorial plane (which

Table 1. Ion-Neutral Reaction Cross Sections

Reaction	$\sigma(15)^a$	$\sigma(26)^a$	Source
$H^+ + H_2O \rightarrow H + H_2O^+$	49	42	<i>Lindsay et al.</i> [1997]
$O^+ + H_2O \rightarrow O + H_2O^+$	41	36	<i>Dressler et al.</i> [2006]
$H_2O^+ + H_2O \rightarrow H_2O + H_2O^+$	10	8.1	<i>Lishawa et al.</i> [1990]
$H_2O^+ + H_2O \rightarrow OH + H_3O^+$	5	1.8	<i>Lishawa et al.</i> [1990]
$OH^+ + H_2O \rightarrow OH + H_2O^+$	10	8.1	Estimate

^a $\sigma(v)$ = cross section at relative velocity, v km s⁻¹, in Å².

is nearly coincident with the rotational equatorial plane since Saturn's dipole tilt is negligible), the ambient plasma conditions in the vicinity of Enceladus' L shell ($L = 4$), as modeled by Sittler et al., are $n_e = 38$ cm⁻³, $T_e = 1$ eV, $n_{H^+} = 3$ cm⁻³, $T_{H^+} = 3$ eV, $n_{W^+} = 35$ cm⁻³, and $T_{W^+} = 36$ eV.

[17] Close to Enceladus, the plasma is slowed because of the interaction with the water plume. In this region, the plasma density increases, although the electrons are still cool. *Tokar et al.* [2006], using observations from CAPS and RPWS, determined that the electron density in the plasma-Enceladus interaction region consists of a cold component with $n_e = 70$ cm⁻³ and $T_e = 1.4$ eV, and a hot component with $n_e = 0.2$ cm⁻³ and $T_e = 12.5$ eV. Although the absolute ion abundances have not been determined from these data, the relative abundances of the major water group ions are approximately equal. Assuming charge neutrality in the plasma ($n_i = n_e$), and a n_{W^+}/n_{H^+} ratio equal to that far from Enceladus, then $n_{O^+} \sim n_{OH^+} \sim n_{H_2O^+} \sim n_{H_3O^+} \sim 16$ cm⁻³, and $n_{H^+} \sim 6$ cm⁻³.

[18] Neutrals escaping from Enceladus are lost through interactions with magnetospheric plasma and solar UV photons. Tables 1, 2, and 3 list the ion-neutral (including charge exchange), electron impact, and photo reactions included in our model. The individual neutral species are assumed not to interact. The dominant loss processes are ion-neutral reactions between escaping neutrals and ambient plasma ions and photo-dissociation by solar UV radiation.

[19] Ion-neutral reaction rates depend on the relative velocities of the neutrals and ions in the magnetosphere:

$$\nu = \sigma v(r) n_i \quad (3)$$

where ν is the reaction rate in s⁻¹, σ is the interaction cross section, n_i is the ion density, and $v(r) = |\mathbf{v}_i - \mathbf{v}_n|$ is the relative speed between the ion and neutral species. Assuming that the plasma is rigidly corotating, the ion speed is $v_i = \Omega \rho$ where $\Omega = 1.62 \times 10^{-4}$ s⁻¹ [*Sánchez-Lavega*, 2005] is

Saturn's rotation rate and ρ is the cylindrical distance from Saturn's rotational axis. At Enceladus, the ion speed is 38.6 km/s. Neutral velocities are tracked in the model, but for comparison, Enceladus' orbital speed is 12.6 km/s, and the speed of the plasma relative to Enceladus is 26.0 km/s. *Johnson et al.* [2006] have shown that the presence of H₃O⁺ ions in the magnetosphere implies that the flow velocity near Enceladus must be slower than the magnetospheric corotation velocity. This conclusion is consistent with CAPS observations showing slowing and deflection of the plasma by the injection of pickup ions [*Tokar et al.*, 2006]. We estimate the magnitude of the velocity perturbation on the basis of our modeled Enceladus source in section 3.

[20] Photo-reaction rates are given at 1 AU by *Huebner et al.* [1992]. These rates are inversely proportional to the distance to the sun squared and are constant across the Saturnian system. In modeling photo processes, we have assumed the sun is in a "quiet" state. Because the production of pickup ions is dominated by charge exchange processes, solar variability has little effect on the overall mass loading rate. Although photoionization is not an important water loss process, photodissociation of H₂O to create neutral OH and H is approximately equal in importance to ion-neutral reactions, with the rate 1.1×10^{-7} s⁻¹ for the quiet sun. Variations in solar UV flux may affect the morphology of the neutral water torus, but in the region close to Enceladus we are interested in here, this difference is not important.

[21] The ionization and dissociation rates for electron impact processes are computed by

$$\nu = n_e \times \kappa(T_e) \quad (4)$$

where n_e is the electron density, and κ is the rate coefficient in cm³ s⁻¹ as a function of the electron temperature T_e . The rate coefficient is determined by $\int \sigma(v) f(v) dv$, where $f(v)$ is

Table 2. Photo-Reaction Rates at 9.5 AU^a

Reaction	Rate Coefficient (s ⁻¹) ^b	Mass Loading ^c
$H_2O + h\nu \rightarrow OH + H$	$1.1 \times 10^{-7} - 2.0 \times 10^{-7}$	No
$H_2O + h\nu \rightarrow H_2 + O$	$6.6 \times 10^{-9} - 1.6 \times 10^{-8}$	No
$H_2O + h\nu \rightarrow H + H + O$	$8.3 \times 10^{-9} - 2.1 \times 10^{-8}$	No
$H_2O + h\nu \rightarrow H_2O^+ + e$	$3.6 \times 10^{-9} - 9.1 \times 10^{-9}$	Yes
$H_2O + h\nu \rightarrow H + OH^+ + e$	$6.1 \times 10^{-10} - 1.6 \times 10^{-9}$	Yes
$H_2O + h\nu \rightarrow H_2 + O^+ + e$	$6.4 \times 10^{-11} - 2.4 \times 10^{-10}$	Yes
$H_2O + h\nu \rightarrow OH + H^+ + e$	$1.4 \times 10^{-10} - 4.5 \times 10^{-10}$	Yes
$H_2O + h\nu \rightarrow$ all reactions	$1.3 \times 10^{-7} - 2.5 \times 10^{-7}$	
$H_2O + h\nu \rightarrow$ mass loading reactions	$4.4 \times 10^{-9} - 1.1 \times 10^{-8}$	

^aSource, *Huebner et al.* [1992].

^bRange gives variation between "Quiet Sun" and "Active Sun" from *Huebner et al.* [1992].

^cMass-loading reactions are those with an ion as a product.

Table 3. Electron Impact Reaction Rate Coefficients^a

Reaction	$\kappa(1.5 \text{ eV})^b$	$\kappa(12.5 \text{ eV})^b$	Mass-Loading? ^c
$\text{H}_2\text{O} + e \rightarrow \text{OH} + \text{H}$	8.3×10^{-11}	2.0×10^{-8}	No
$\text{H}_2\text{O} + e \rightarrow \text{H}_2\text{O}^+ + 2e$	7.6×10^{-13}	1.2×10^{-8}	Yes
$\text{H}_2\text{O} + e \rightarrow \text{OH}^+ + \text{H} + 2e$	3.9×10^{-15}	2.5×10^{-9}	Yes
$\text{H}_2\text{O} + e \rightarrow \text{O}^+ + \text{H}_2 + 2e$	7.3×10^{-15}	1.6×10^{-10}	Yes
$\text{H}_2\text{O} + e \rightarrow \text{H}^+ + \text{OH} + 2e$	4.9×10^{-16}	1.1×10^{-9}	Yes
$\text{H}_2\text{O} + e \rightarrow \text{mass loading reactions}$	7.7×10^{-13}	1.6×10^{-8}	

^aSource, *Itikawa and Mason* [2005].

^b $\kappa(T_e)$ = rate coefficient at electron temperature T_e in $\text{cm}^{-3} \text{s}^{-1}$.

^cMass-loading reactions are those with an ion as a product.

a Maxwellian distribution of the measured electron temperature, and σ is the experimentally determined cross section. Cross sections for electron impact dissociation and ionization are reviewed by *Itikawa and Mason* [2005]. The dominant reaction is the ionization reaction $\text{H}_2\text{O} + e \rightarrow \text{H}_2\text{O}^+ + 2e$. Despite the fact that the cool component of the electron distribution function dominates the density, the hot electrons do most of the ionizing. This is because the ionization and dissociative ionization cross sections are negligible for $T_e < 10 \text{ eV}$ and increase rapidly for $T_e > 10 \text{ eV}$. Because of this hot component, the total electron impact ionization and dissociative ionization rate is $\sim 3 \times 10^{-9} \text{ s}^{-1}$. The dominant measured dissociation reaction is for the creation of OH and H in their ground states. The production of ground state atomic oxygen has not been measured, although it may be significant since the minimum energy required for the reaction (5.03 eV) is comparable to that required for production of OH (5.10 eV).

2.3. Neutral Source Rate

[22] Because the electron and ion densities are small, little neutral loss occurs in the exosphere of Enceladus. The timescale for H_2O destruction is ~ 500 hours; water molecules traveling at 0.5 km/s can travel $50 R_{\text{En}}$ in only 7 hours. Therefore the initial conditions are the primary factor in determining the distribution of exospheric neutrals.

[23] We model the INMS observations as the sum of an exosphere produced from a distributed source which because of the lack of constraints, we treat as spatially uniform ejection from the surface, a plume centered on the south pole, and a background water torus. The background is composed of water molecules which have escaped from Enceladus and spread out in orbit around Saturn to form a narrow, roughly longitudinally symmetric torus centered on Enceladus' orbit [*Johnson et al.*, 2006]. The background level is a function of the source rate from Enceladus, although uncertainties in the plasma prevent the density from being well constrained. We consider the background level to be a free parameter, although we will present a comparison between the model fit and the expected background level on the basis of the determined plume source rate.

[24] The spatially uniform source produces a spherically symmetric exosphere within the Hill sphere, the region in which the satellite's gravity dominates over the central planet's gravity. For a satellite such as Enceladus, where material ejected from the surface freely escapes with no ionization, dissociation, or significant gravitational perturbation from the satellite, the density drops off with distance proportional to r^{-2} . Deviations from an observed r^{-2}

density profile are due either to a non-isotropic surface distribution or a significant slow (i.e., less than escape velocity) component to the isotropic loss. We assume that the production mechanism for this component is a process like sputtering with a velocity distribution given in equation (2). This choice of velocity distribution does not affect our results as the INMS data are consistent with any mechanism which produces water with velocity greater than escape velocity.

[25] The portion of the in situ INMS water vapor observations after closest approach (during which the subsurface point of the spacecraft was moving northward from -22°) is consistent with isotropic escape from the surface. Figure 2 shows that the outbound (northern) portion of Cassini's flyby is well fit by a distributed source with a strength of $8 \times 10^{25} \text{ H}_2\text{O/s}$, if we assume a global source and use a background torus density $\sim 1.6 \times 10^4 \text{ cm}^{-3}$. Both this global source rate and the background are higher than the previously estimated surface sputtering rates [*Richardson et al.*, 1998; *Jurac et al.*, 2001; *Jurac and Richardson*, 2005]; although, the larger background may be consistent with the additional source to the water torus from the plume. To find this result, the data have been fit to the function:

$$n_{\text{data}} = \text{background} + \left(\frac{\text{source}}{10^{26}}\right) \times \text{model fit} \quad (5)$$

where $\text{model fit} = 10^{5.5} r^{-2.3}$ is the fit to a model of a sputter-like exosphere within $10 R_{\text{E}}$ of Enceladus with a source of

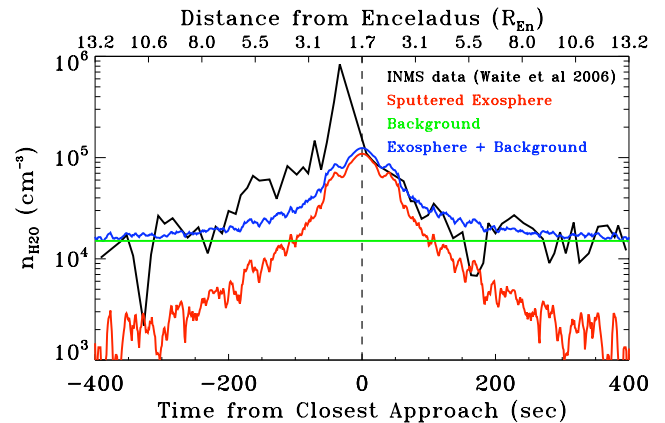


Figure 2. Comparison between isotropic sputtering model of Enceladus' exosphere and the INMS data. The sputtering source rate is $8 \times 10^{25} \text{ H}_2\text{O/s}$.

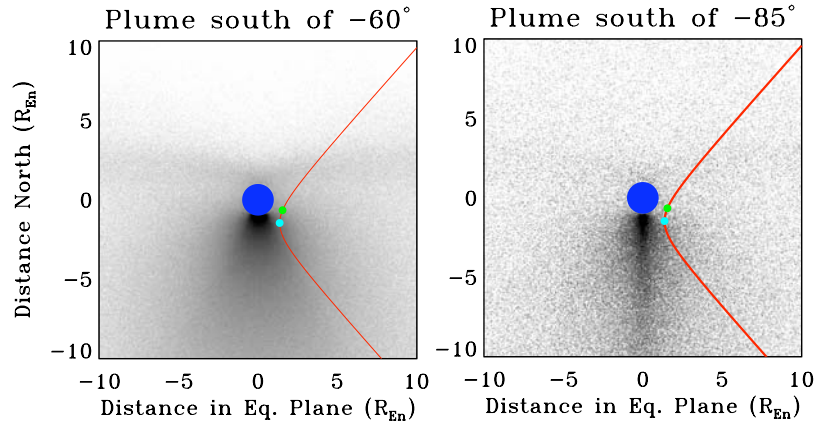


Figure 3. Comparison between plumes formed from different-sized active regions. Left, active region is south of -60° longitude. Right, active region south of -85° . The blue circle represents Enceladus' disk. The red line shows Cassini's trajectory in cylindrical coordinates (z versus $\sqrt{x^2 + y^2}$). The green dot shows the Enceladus closest approach; the light blue dot marks the point of maximum water density measured by INMS.

10^{26} $\text{H}_2\text{O}/\text{s}$. The deviation of this fit from a true r^{-2} dependence is due to the influence of Saturn's gravity outside the Hill sphere.

[26] This global component to Enceladus' atmosphere is consistent with the stellar occultation measurements. The occultation of λ Sco, as well as the egress of γ Ori from behind Enceladus, failed to detect water vapor absorption. These three observations occurred at latitudes north of -30° , in regions dominated by the distributed component of the exosphere. The column density through a line tangent to the surface of Enceladus is $\sim 2 \times 10^{13} \text{ cm}^{-2}$ in our sputtering model, significantly lower than the UVIS detection limit of $\sim 10^{15} \text{ cm}^{-2}$. Therefore UVIS could not detect the putative global component of Enceladus' atmosphere.

[27] The inbound ($t < 0$) portion of the INMS data is not consistent with a global atmospheric source. This portion of the INMS data can be divided into two sections, for $t < -60$ s, where the rise in H_2O density is faster than that expected by the global source and $-60 < t < 0$ s, which corresponds with the sharp spike in water density. These features in the density profile require a local source or sources.

[28] The ingress of γ Ori observed by UVIS currently offers the best view of the water vapor plume. The ingress point was at -76° , but because Cassini was over Enceladus' southern hemisphere, the star passed directly over the south pole, and the observed water column increased consistently until the star was blocked by the surface. We model the plume using localized sources with uniform ejection from regions centered on the south pole and normalize to the source rate needed to match the observed surface column density (Figure 3). The source rate decreases from 1.5×10^{28} to $0.6 \times 10^{28} \text{ H}_2\text{O}/\text{s}$ as the active area shrinks from the region south of -60° to -85° because of the increased flux density for a given source rate as the size of the region decreases. These results are consistent with the source rate estimate of $0.5\text{--}1.0 \times 10^{28} \text{ H}_2\text{O}/\text{s}$ made by Hansen *et al.* [2006] on the basis of the observed column density and assumptions of gas velocity and cross-sectional plume area.

[29] To simultaneously model the UVIS and INMS results, the plume must be confined to regions southward of approximately -80° . For larger active regions, the source rates consistent with the INMS data are two orders of magnitude lower than that implied by our modeling of the UVIS observations. This implies that only a small fraction of the material from the plume was intercepted by Cassini as it flew past Enceladus. As shown in Figure 3, a plume from a small region centered on the south pole largely misses the Cassini trajectory. A wider plume sends material over a much larger volume near Enceladus. A narrow plume is also consistent with the fast decrease in density observed by UVIS as the star traversed the plume. We are not able to produce an entirely consistent fit to the simultaneous UVIS and INMS observations because of the small number of observations, unknown source mechanism, and likely complex nature of the source region or regions. We have assumed a uniform source over a region of Enceladus' surface and an angular distribution consistent with sublimation of ice. This does not take into account ISS observations suggesting the dust streams coincide with the tiger stripes by Porco *et al.* [2006] or any local surface effects. For example, a narrow jet, unobserved by UVIS, could account for the peak in the INMS data. We have, however, been able to constrain the source rate and size of the active region through our technique.

3. Computing the Mass Loading Rate

[30] As discussed above, we have used the INMS data along with the surface value of the UVIS data to show that there are two components to the plume, a distributed component and a plume which was sufficiently narrow that INMS saw only the edge of it. Although we have not fully described the latter, we can use these models to discuss the neutral cloud interaction with the local plasma. We determine the mass loading rate of the magnetosphere by estimating the ion production rate when the model plumes interact with the plasma observed by Cassini. We assume the plasma conditions described in section 2.2. The total

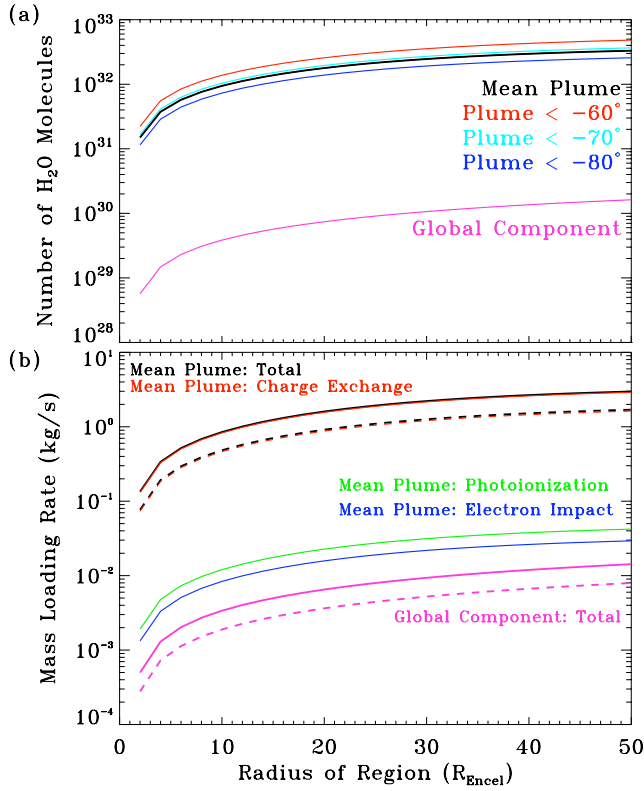


Figure 4. (a) Number of water molecules within a sphere centered on Enceladus for the plume models shown in Figure 3, as well as for the global component with a source rate of 8×10^{25} H₂O/s. The geometry of the plume does not significantly affect the number of molecules; the result depends only on the source rate from the surface. A nominal source rate of 10^{28} H₂O/s is shown in black. (b) Mass loading rates due to charge exchange, electron impact ionization, and photo-ionization versus radius of a sphere centered on Enceladus for the mean plume and global exosphere. The solid lines for the mean plume and global total mass loading rate assume a relative ion-neutral velocity of 26 km/s; broken lines assume 15 km/s.

mass loading rate is the sum of the rates of the individual ion-neutral (including charge exchange), photo-ionization, and electron-impact ionization reactions. Mass loading reactions are those which produce a fresh ion; therefore, dissociation is not relevant for this discussion. Charge exchange reactions are included as they produce new ions at rest relative to Enceladus and result in a change in the total plasma momentum. They do not increase the total plasma content, since an ion is lost for each new one created, but the acceleration of the fresh ion to full corotational velocity is detected by its effect on the plasma flow and magnetic field. The total mass loading rate, \dot{M} , is:

$$\dot{M} = \sum \dot{M}_{\text{IN}} + \sum \dot{M}_{\text{Photo}} + \sum \dot{M}_{\text{EI}} \quad (6)$$

where \dot{M}_{IN} , \dot{M}_{Photo} , and \dot{M}_{EI} are the individual ion-neutral, photo-ionization, and electron impact mass loading rates, respectively.

[31] Ion-neutral reaction rates depend on the densities of the reactants, the relative velocities, and the velocity dependent cross sections. For reactions in the form $A^+ + B \rightarrow C + D^+$ (for charge exchange, $A = C$ and $B = D$), the total ion-neutral mass loading rate is:

$$\dot{M}_{\text{IN}} = \sum_j \left(\int_{\text{region}} m_D^j n_A^j n_B^j \sigma^j(v_{\text{rel}}) v_{\text{rel}} dV \right) \quad (7)$$

where the sum is taken over each of the reactions listed in Table 1, and the integral is performed over the region of interest. Using the assumption that the plasma is uniform over the region and that the ejection velocity from Enceladus is small compared with the orbital velocity, equation (7) can be expressed as:

$$\dot{M}_{\text{IN}} = N_{\text{H}_2\text{O}} \times \sum_j \sigma_j m_D^j n_A^j v_{\text{rel}} \quad (8)$$

where $N_{\text{H}_2\text{O}}$ is the total number of water molecules in the region as determined from the model calculations.

[32] The mass loading rate due to photoionization is given by:

$$\dot{M}_{\text{photo}} = \sum_j (m_j \kappa_j) \times N_{\text{H}_2\text{O}} \quad (9)$$

where the reactions considered for photoionization of water are listed in Table 2. The ions produced through photoionization are H₂O⁺, OH⁺, O⁺, and H⁺. Because the photoionization rate coefficients are constant across Saturn's magnetosphere, the mass loading rate depends only on the number of neutral water molecules:

$$\dot{M}_{\text{photo}} = 1.3 \times 10^{-34} N_{\text{H}_2\text{O}} \text{ kg s}^{-1} \quad (10)$$

[33] Mass loading due to electron impact ionization depends on both the number of neutrals and the state of the electrons in the magnetosphere (both the density, n_e , and temperature, T_e). Because the thermal plasma is cool ($T_{e,\text{cold}} \sim 1$ eV), the ionization rate primarily depends on the hot electron population, despite its low abundance. Table 3 lists the electron impact reactions which contribute to mass loading. The mass loading rate is:

$$\dot{M}_{\text{EI}} = \sum_j \int_{\text{region}} (m_i^j n_{e,\text{cold}} n_n^j \kappa(T_{e,\text{cold}}) + m_i^j n_{e,\text{hot}} n_n^j \kappa(T_{e,\text{hot}})) dV \quad (11)$$

where m_i^j is the mass of the pickup ion produced by electron impact of neutrals with density n_n^j by reaction j . To first order, the electrons are uniformly distributed over the region occupied by the neutrals, so that $n_{e,\text{cold}}$, $n_{e,\text{hot}}$, and κ are constant over the region, and the mass loading rate can be estimated by

$$\dot{M}_{\text{EI}} = 8.9 \times 10^{-35} N_{\text{H}_2\text{O}} \text{ kg s}^{-1} \quad (12)$$

[34] Figure 4 shows the total number of water molecules and the mass loading rates within a sphere centered on

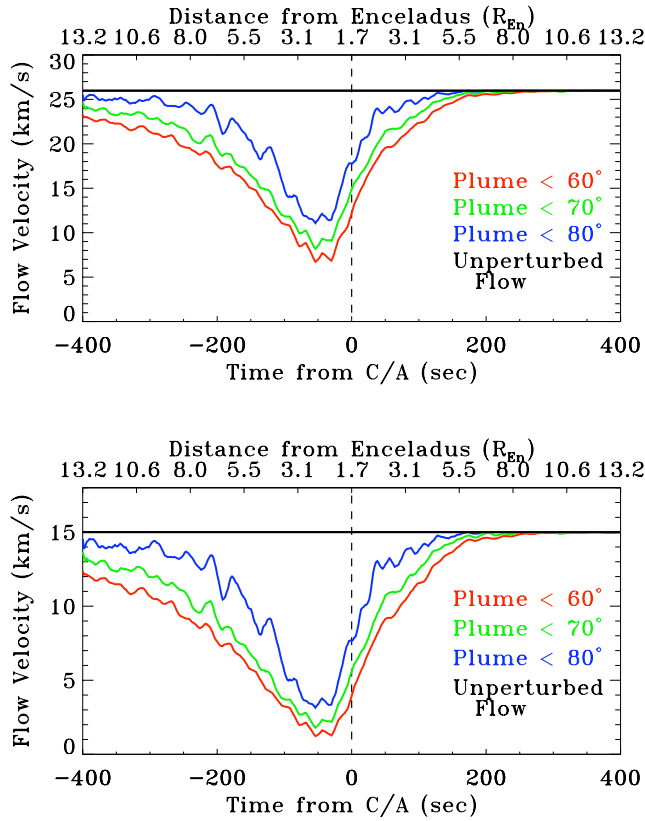


Figure 5. (a) Predicted perturbation in plasma flow velocity for different plume models. The solid black line indicates the corotational velocity relative to Enceladus. (b) Same as Figure 5a but assumes that the plasma has been slowed to 15 km/s relative to Enceladus prior to encountering the plume.

Enceladus as a function of distance from Enceladus (or radius of the sphere). Two cases are shown, the solid lines assume the plasma density measured by Cassini during the Enceladus flyby but with full corotational velocity. The broken lines take into account the velocity perturbation measured by CAPS which indicates that the plasma is slowed upstream of Enceladus and flows through the plume at ~ 15 km/s. As shown below, the plume does not provide enough material to the upstream regions to account for this slowing, implying CAPS observed a separate interaction. Within $50 R_{\text{En}}$, $\sim 2\text{--}3$ kg/s of fresh ions are produced. An upper limit on the effect of the distributed source is found by assuming it is global with a source rate two orders of magnitude lower than the plume. The contribution to the total mass loading rate due to this source is negligible.

[35] An approximate source rate of 10^{28} $\text{H}_2\text{O}/\text{s}$ is used to calculate the mass loading rate. As shown in Figure 3, the source rate we determined depends on the size of the source region. However, the total number of water molecules in the mass loading region depends more strongly on the source rate than the source size. The uncertainties in the size of the plume, time variability of the plume, and the relative speed of the neutrals and ions limit the precision of our result. The mass loading rate is linearly proportional to the source rate, and future observations of Enceladus will allow us to

determine the mass loading rate and plume geometry more accurately.

[36] The injection of fresh pickup ions induces a perturbation in the ion velocities from full magnetospheric corotation. The amount of slowing can be traced to the impulse experienced by the flow as the pickup ions are accelerated by the rotational electric field. By integrating along a fluid element of the flow past Enceladus to the observation site (i.e., the spacecraft location), one gets the following for the change in flow velocity:

$$\Delta v = \int_{-\infty}^{y_0} \left(\frac{1}{\rho} \right) \left(\frac{d\rho_{\text{pu}}}{dt} \right) dy \quad (13)$$

where $\rho = \sum m_{\text{ion}} n_{\text{ion}}$ is the ion mass density of the ambient plasma plus pickup ions, and $v \frac{d\rho_{\text{pu}}}{dt}$ is the impulse term due to pickup ions across the length element $dy \approx v dt$, such that:

$$\frac{d\rho_{\text{pu}}}{dt} = \sum_j m_D^j n_A^j n_{\text{H}_2\text{O}} v(y) \sigma^j(v(y)) \quad (14)$$

The integral is performed along the direction of the magnetic field rotation from an upstream point where neutral density is negligible to the spacecraft location. Charge exchange reactions dominate the impulse term and ensure that the mass density, ρ , remains approximately constant. $v(y) = v_{\text{rel}} - dv$ gives the relative speed between ions, initially corotating and subsequently slowed, and neutrals in Keplerian orbits around Saturn. As the plasma slows, the plasma density increases conserve flux tube content such that $n \times v \sim \text{constant}$. Therefore, for the calculation, we treat the ambient plasma velocity and density as constant. Because the cross sections increase as the velocity decreases, our estimate provides a lower limit on the magnitude of the slowing.

[37] We have ignored the increase in plasma pressure because of ion pickup which we estimate to be less than 10%, Alfvén wave generation, and field-aligned currents which close with Saturn’s ionosphere. The Alfvén wave propagation time (~ 10 min) is comparable to the time for the flow to pass through the Enceladus plume, so Saturn’s ionospheric current is important as discussed in *Pontius and Hill* [2006]. This latter effect means our expression is equivalent to the pickup current discussed by *Goertz* [1980] which then closes via field-aligned currents through Saturn’s ionosphere. We also relegate the effects of pile up as the flow slows down, compression of field lines, and tension in the field as it flows past Enceladus for a subsequent paper.

[38] Cassini was upstream of Enceladus on its approach, and therefore did not have optimal geometry to detect ion depletion from the plume. A strong deflection is predicted, however, close to Enceladus (Figure 5) where the flow speed decreases to ~ 10 km/s relative to Enceladus. The magnitude of the velocity perturbation decreases as the plume size decreases since less water is spread to the region upstream of Enceladus. The spacecraft was moving northward during the encounter, so the southward-directed plume has less effect on the outbound trajectory. The maximum deflection associated with the isotropic component is 0.1 km/s.

[39] This prediction is not consistent with the flow deflection observations by CAPS [Tokar *et al.*, 2006]. CAPS measured the plasma flow velocity from 15 to 10 min before closest approach and from ~ 20 to 30 min after closest approach; the perturbation was detected $\sim 27 R_{\text{En}}$ from Enceladus. The plume models most consistent with the neutral water gas measurements do not produce sufficient water to directly cause the measured perturbation. We do not predict a velocity perturbation because of the plasma interaction with the plume until ~ 5 min before closest approach, at which time CAPS had no data due to spacecraft pointing constraints. A possible explanation is that CAPS observed charge exchange associated with the Enceladus neutral torus discussed by Johnson *et al.* [2006], although we have not estimated the effect of a longitudinally symmetric torus. If the plasma is slowed prior to encountering the plume, the interaction will further slow the plasma to 5 km/s (Figure 5b). A more complete discussion of the CAPS observations will be left for a future work on the interaction between Enceladus, the water tori, and Saturn's magnetosphere.

4. Summary and Conclusions

[40] The discovery of geologic activity at Enceladus has profound implications for the material in Saturn's magnetosphere. On the basis of the estimates above, which are consistent with the Enceladus source rates needed to supply the secondary OH torus [Johnson *et al.*, 2006; Jurac *et al.*, 2002; Jurac and Richardson, 2005], the small icy moon emits ~ 300 kg/s of water from its south pole, most of which is distributed around Saturn either as neutral H₂O gas, ice grains in the E ring, or as plasma trapped in Saturn's magnetic field. We have shown that the gas plume observed by the instruments on Cassini is consistent with a two-component source from Enceladus, with more than 99% of the material associated with the south polar plume. The remaining water is consistent with a global source of a 2–3 kg/s.

[41] Interaction between the water gas plume and the magnetospheric plasma produces ~ 3 kg/s of fresh water group ions which are then picked up by the magnetosphere, consistent with estimates of the mass loading rate from the Cassini/MAG experiment. The flow speed would have been expected to decrease to ~ 10 km/s near the closest approach to the south pole during the 14 July 2005 flyby. These results are not consistent with deflection measured by the CAPS experiment, although the magnitude of the flow deflection is consistent, CAPS detected plasma slowdown much farther from Enceladus than we predict. This may indicate a neutral population farther from Enceladus that is fed by the plume, although physically separate.

[42] **Acknowledgments.** Wolfgang Baumjohann thanks the reviewers for their assistance in evaluating this paper. MHB is supported through the NASA Postdoctoral Program.

References

- Brown, M. E., and R. E. Hill (1996), Discovery of an extended sodium atmosphere around Europa, *Nature*, *380*, 229–231.
- Burger, M. H. (2003), Io's neutral clouds: From the atmosphere to the plasma torus, Ph.D. thesis, University of Colorado, Boulder, Colorado.
- Burger, M. H., and R. E. Johnson (2004), Europa's neutral cloud: Morphology and comparisons to Io, *Icarus*, *171*, 557–560.
- Dougherty, M. K., K. K. Khurana, F. M. Neubauer, C. T. Russell, J. Saur, J. S. Leisner, and M. E. Burton (2006), Identification of a dynamic atmosphere at Enceladus with the Cassini magnetometer, *Science*, *311*, 1406–1409.
- Dressler, R. A., M. J. Bastian, D. J. Levandier, and E. Murad (2006), Empirical model of the state-state dynamics in near-resonant hyperthermal X⁺ + H₂O charge-transfer reactions, *Int. J. Mass Spectrom.*, *159*, 245–256.
- Goertz, C. K. (1980), Multiscale periodic structure in the Io wake, *J. Geophys. Res.*, *85*, 2949–2956.
- Hall, D. T., et al. (1995), Detection of an oxygen atmosphere on Jupiter's moon Europa, *Nature*, *373*, 677–679.
- Hall, D. T., P. D. Feldman, J. B. Holberg, and M. A. McGrath (1996), Fluorescent hydroxyl emissions from Saturn's ring atmosphere, *Science*, *272*, 516–518.
- Hansen, C. J., L. Esposito, A. I. F. Stewart, J. Colwell, A. Hendrix, W. Pryor, D. Shemansky, and R. West (2006), Enceladus' water vapor plume, *Science*, *311*, 1422–1425.
- Huebner, W. F., J. J. Keady, and S. P. Lyon (1992), Solar photo rates for planetary atmospheres and atmospheric pollutants, *Astrophys. Space Sci.*, *195*, 1–289.
- Ip, W.-H. (1986), The sodium exosphere and magnetosphere of Mercury, *Geophys. Res. Lett.*, *13*, 423–426.
- Itikawa, Y., and N. Mason (2005), Cross sections for electron collisions with water molecules, *J. Phys. Chem. Ref. Data*, *34*, 1.
- Johnson, R. E. (1990), *Energetic Charged-Particle Interactions with Atmospheres and Surfaces*, X, 232 pp., Springer, New York.
- Johnson, R. E., M. K. Pospieszalska, E. M. Sieveka, A. F. Cheng, L. J. Lanzerotti, and E. C. Sittler (1989), The neutral cloud and heavy ion inner torus at Saturn, *Icarus*, *77*, 311–329.
- Johnson, R. E., T. I. Quickenden, P. D. Cooper, A. J. McKinley, and C. G. Freeman (2004), The production of oxidants in Europa's surface, *Astrobiology*, *3*, 823–850.
- Johnson, R. E., et al. (2006), The Enceladus and OH Tori at Saturn, *Astrophys. J. Lett.*, *644*, L137–L139.
- Jurac, S., and J. D. Richardson (2005), A self-consistent model of plasma and neutrals at Saturn: Neutral cloud morphology, *J. Geophys. Res.*, [Space Phys.], *110*, 9220.
- Jurac, S., R. E. Johnson, J. D. Richardson, and C. Paranicas (2001), Satellite sputtering in Saturn's magnetosphere, *Planet. Space Sci.*, *49*, 319–326.
- Jurac, S., M. A. McGrath, R. E. Johnson, J. D. Richardson, V. M. Vasyliunas, and A. Eviatar (2002), Saturn: Search for a missing water source, *Geophys. Res. Lett.*, *29*(24), 2172, doi:10.1029/2002GL015855.
- Kivelson, M. G. (2006), Does Enceladus govern magnetospheric dynamics at Saturn?, *Science*, *311*, 1391–1392.
- Khurana, K. K., M. K. Dougherty, C. T. Russell, and J. S. Leisner (2007), Mass loading of Saturn's magnetosphere near Enceladus, *J. Geophys. Res.*, doi:10.1029/2006JA012110, in press.
- Lindsay, B. G., D. R. Sieglaff, K. A. Smith, and R. F. Stebbings (1997), Charge transfer of 0.5-, 1.5-, and 5-keV protons with H₂O: Absolute differential and integral cross sections, *Phys. Rev. A*, *55*, 3945–3946.
- Lishawa, C. R., R. A. Dressler, J. A. Gardner, R. H. Salter, and E. Murad (1990), Cross sections and product kinetic energy analysis of H₂O⁺-H₂O collisions at suprathreshold energies, *J. Chem. Phys.*, *93*, 3196–3206.
- Persoon, A. M., et al. (2005), Equatorial electron density measurements in Saturn's inner magnetosphere, *Geophys. Res. Lett.*, *32*, L23105, doi:10.1029/2005GL024294.
- Pontius, D. H., and T. W. Hill (2006), Enceladus: A significant plasma source for Saturn's magnetosphere, *J. Geophys. Res.*, *111*, A09214, doi:10.1029/2006JA011674.
- Porco, C. C., et al. (2006), Cassini observes the active south pole of Enceladus, *Science*, *311*, 1393–1401.
- Pospieszalska, M. K., and R. E. Johnson (1991), Micrometeorite erosion of the main rings as a source of plasma in the inner Saturnian plasma torus, *Icarus*, *93*, 4552.
- Richardson, J. D. (1998), Thermal plasma and neutral gas in Saturn's magnetosphere, *Rev. Geophys.*, *36*, 501–524.
- Richardson, J. D., A. Eviatar, M. A. McGrath, and V. M. Vasyliunas (1998), OH in Saturn's magnetosphere: Observations and implications, *J. Geophys. Res.*, *103*, 20245–20256.
- Sánchez-Lavega, A. (2005), How long is the day on Saturn?, *Science*, *307*, 1223–1224.
- Saur, J., and D. F. Strobel (2005), Atmospheres and plasma interactions at Saturn's largest inner icy satellites, *Astrophys. J.*, *620*, L115–L118.
- Shemansky, D. E., P. Matheson, D. T. Hall, H.-Y. Hu, and T. M. Tripp (1993), Detection of the hydroxyl radical in the Saturn magnetosphere, *Nature*, *363*, 329–331.
- Shi, M., R. A. Baragiola, D. E. Grosjean, R. E. Johnson, S. Jurac, and J. Schou (1995), Sputtering of water ice surfaces and the production of extended neutral atmospheres, *J. Geophys. Res.*, *100*, 26,387–26,396.

- Sittler, E. C., et al. (2004), Pickup ions at Dione and Enceladus: Cassini Plasma Spectrometer simulations, *J. Geophys. Res.*, *109*, A01214, doi:10.1029/2002JA009647.
- Sittler, E. C., et al. (2005a), Preliminary results on Saturn's inner plasma-sphere as observed by Cassini: Comparison with Voyager, *Geophys. Res. Lett.*, *32*, L14S07, doi:10.1029/2005GL022653.
- Sittler, E. C., et al. (2005b), Ion source rate within Saturn's inner magnetosphere: Cassini results, *Bull. Am. Astron. Soc.*, *37*, 758.
- Sittler, E. C., et al. (2006), Cassini observations of Saturn's inner plasma-sphere: Saturn orbit insertion results, *Planet. Space Sci.*, *54*, 1197–1210.
- Smith, H. T., M. Shappirio, E. C. Sittler, D. Reisenfeld, R. E. Johnson, R. A. Baragiola, F. J. Crary, D. J. McComas, and D. T. Young (2005), Discovery of nitrogen in Saturn's inner magnetosphere, *Geophys. Res. Lett.*, *32*, L14503, doi:10.1029/2005GL022654.
- Spencer, et al. (2006), Cassini encounters Enceladus: Background and the discovery of a south polar hot spot, *Science*, *311*, 1401–1405.
- Tokar, R. L., et al. (2006), The interaction of the atmosphere of Enceladus with Saturn's plasma, *Science*, *311*, 1409.
- Waite, J. H., et al. (2006), Cassini ion and neutral mass spectrometer: Enceladus plume composition and structure, *Science*, *311*, 1419–1422.
- Young, D. T., et al. (2005), Composition and dynamics of plasma in Saturn's magnetosphere, *Science*, *307*, 1262–1266.

M. H. Burger and E. C. Sittler Jr., Goddard Space Flight Center, NASA, Greenbelt, MD, USA. (mburger@pop600.gsfc.nasa.gov)

R. E. Johnson, H. T. Smith, and O. J. Tucker, University of Virginia, Charlottesville, VA, USA.

V. I. Shematovich, Department of Stellar Physics and Evolution, Institute of Astronomy, Russian Academy of Sciences, Moscow, Russia.